

## Minimal Functional Clusters Predict the Probability of Reentry in Cardiac Fibrotic Tissue

Farhad Pashakhanloo<sup>1,\*</sup> and Alexander V. Panfilov<sup>2,3,4</sup>

<sup>1</sup>Cardiovascular Division, Beth Israel Deaconess Medical Center, Harvard Medical School, Boston, Massachusetts 02215, USA

<sup>2</sup>Department of Physics and Astronomy, Ghent University, Krijgslaan 281, Ghent, 9000, Belgium

<sup>3</sup>Ural Federal University, 620002 Ekaterinburg, Russia

<sup>4</sup>World-Class Research Center “Digital biodesign and personalized healthcare”, Sechenov University, 119146 Moscow, Russia



(Received 4 December 2020; accepted 13 July 2021; published 23 August 2021)

Cardiac fibrosis is a well-known arrhythmogenic condition which can lead to sudden cardiac death. Physically, fibrosis can be viewed as a large number of small obstacles in an excitable medium, which may create nonlinear wave turbulence or reentry. The relation between the specific texture of fibrosis and the onset of reentry is of great theoretical and practical importance. Here, we present a conceptual framework which combines functional aspects of propagation manifested as conduction blocks, with reentry wavelength and geometrical clusters of fibrosis. We formulate them into the single concept of minimal functional cluster and through extensive simulations show that it characterizes the path of reexcitation accurately, and importantly its size distribution quantitatively predicts the reentry probability for different fibrosis densities and tissue excitabilities.

DOI: [10.1103/PhysRevLett.127.098101](https://doi.org/10.1103/PhysRevLett.127.098101)

**Introduction.**—Propagating nonlinear waves of excitation are a widespread phenomenon in physical, chemical, and biological excitable systems [1]. Such waves control many important processes, for example, the initiation of cardiac contraction. Abnormal propagation of these waves in the heart causes life-threatening cardiac arrhythmias [2]. Most such arrhythmias occur when the waves form turbulent rotational activity, or reentry. One of the most well-known pathologies leading to the formation of reentry in cardiac tissue is fibrosis [3,4]. This refers to the presence of a large number of obstacles (nonexcitable cells) dispersed throughout the cardiac tissue. The relation between the pattern of fibrosis and the onset of arrhythmia is of great importance from the basic science perspective as well as in practical cardiology for determining optimal arrhythmia treatments.

From the physical point of view, the presence of fibrosis could contribute to rotational activity in multiple ways. Globally, for a rotation to be sustained, its period must be longer than the refractory time. This is because, after the excitation, cardiac cells need recovery time and can be reexcited only after this refractory period is over. If this temporal condition is considered in the spatial domain, it suggests that the wavelength of the rotational activity cannot be smaller than the product of the wave velocity ( $v$ ) and the refractory period ( $t_r$ ). The presence of a large structural heterogeneity such as clusters of fibrosis, thus, can provide a natural geometric structure around which such rotation can occur (see Fig. S1 [5]). In most cases, the initiation of reentry requires an additional condition, called unidirectional block [6]. In this situation, the wave propagation is locally blocked from one side but is successful

from the opposite direction. Unidirectional blocks can occur due to the structural heterogeneity in the fibrosis, but their occurrence primarily depends on the microscopic geometry and wave properties such as tissue excitability (see Supplemental Material [5] for additional background, which includes Refs. [7–11]).

Both the global and local conditions have been studied with respect to fibrosis. Important work from Alonso and Bär [12] has shown that the reentry probability in fibrotic tissue is strongly correlated with the probability of formation of fibrotic clusters above a typical size. In addition, the idea of a unidirectional block has been considered in many studies on fibrosis as a qualitative mechanism for reentry formation [3,13]. Although the two conditions for formation of reentry (i.e., unidirectional blocks and the critical wavelength) have been well known for more than 100 years [2], they have never been combined together to systematically determine the probability of reentry formation in complex fibrotic tissue.

In this Letter, we introduce the minimal functional cluster, a concept that incorporates the functional characteristics of wave propagation as conduction blocks, as well as the geometrical conditions for formation of reentry. We show that the probability of reentry formation in various excitability regimes can be accurately and quantitatively predicted from the size distribution of these clusters in the tissue.

**Model.**—Details of the model formulation and simulations are presented in Supplemental Material [5]. In short, the model consists of a 2D mesh of  $160 \times 160$  square elements with an edge length of 0.25 mm. Fibrosis was modeled by randomly removing elements from the mesh with probability  $\phi$  (0–0.65,  $N = 250$  realizations per  $\phi$ )

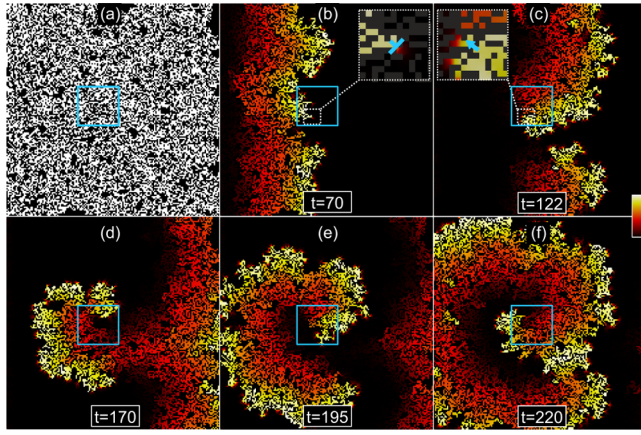


FIG. 1. Action potential wave propagation and reentry formation in tissue with fibrosis. (a) A model with fibrosis (black) at  $\phi = 0.5$ . Snapshots of transmembrane voltage maps following wave initiation at the left boundary at  $t = 0$ : (b) the occurrence of a unidirectional block (marked by the blue  $T$ ), (c) reexcitation of the tissue behind the block (blue arrow), and (d)–(f) formation and persistence of the reentry. The blue box highlights the core area of the reentry.

[Fig. 1(a)]. Simulations of action potential wave propagation and reentry were performed by solving the monodomain equations with a cardiac-specific single-cell model [14]. Experiments were repeated at three levels of tissue excitability ( $e = 1, 0.5$ , and  $0.33$ ). The stimulus was applied from the boundary of the slab to generate planar waves. Reentry was deemed successful if the activation in the tissue lasted  $\geq 450$  ms following the stimulus.

*Conduction blocks and reentry initiation.*—Figures 1(b)–1(f) show a representative case of reentry formation in the model. The macroscopic rotational activity is initiated by a microscopic unidirectional block, where the propagation is blocked from the left direction but is successful from the opposite side. We detected all the microscopic blocks in the tissue following pacing and from those identified the unidirectional blocks by additional pacing from multiple sides (see Supplemental Material [5]).

*Functional clusters.*—The concept of a cluster has been previously defined as a set of connected inexcitable elements forming an obstacle [12]. This is a pure geometric characteristic of the texture, and, in the absence of any conduction blocks, the clusters would solely determine the path of the propagating wave. However, the presence of microscopic blocks modifies the effective connectivity pathway for the wave. In the case of fibrosis-induced conduction blocks, these blocks happen at the junction or close proximity of two or more regions of fibrosis, effectively connecting those fibrotic clusters into a larger cluster of unexcitable tissue that we call a *functional cluster* (see also Supplemental Material [5]). An example of a functional cluster is shown in Fig. 2.

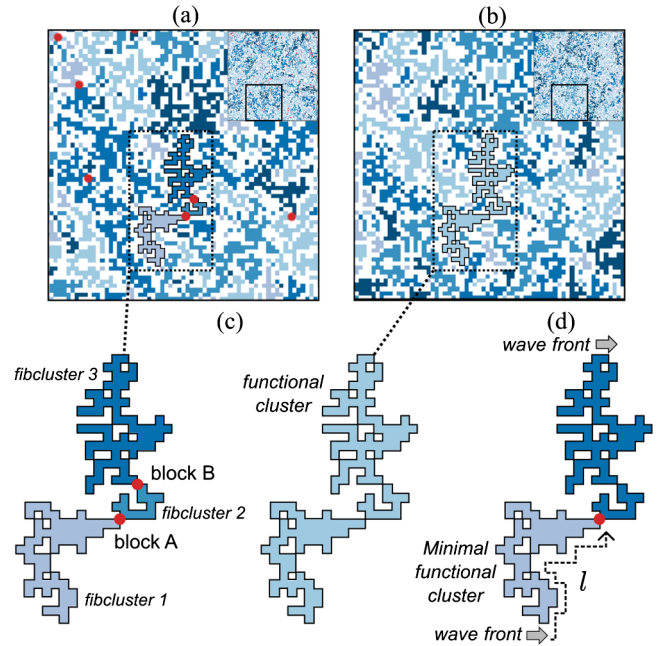


FIG. 2. Formation of functional clusters. (a) Map of randomly color-coded fibrotic clusters superimposed with the locations of the conduction blocks (red circles) following pacing from the left boundary ( $\phi = 0.5$ ,  $e = 0.5$ ). (b) Corresponding map of functional clusters. (c) A representative functional cluster (right) formed from three smaller fibrotic clusters and two conduction blocks (left). (d) Minimal functional cluster (light colored) associated with the unidirectional block A. The dashed line shows the path of reexcitation.

Next, we investigate the statistical properties of functional clusters as a function of  $\phi$  and  $e$ . Figure 3(a) illustrates the distributions of cluster sizes ( $s$ ) using a log-log plot of complementary cumulative distributions function (CCDF), i.e.,  $P(S \geq s)$ . It can be seen that functional clusters follow qualitatively the same form of distribution as fibrotic clusters, which can be approximated

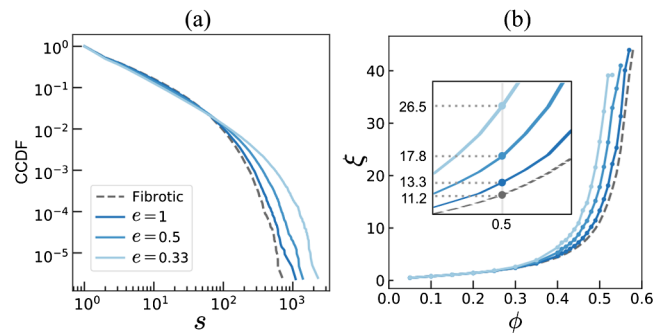


FIG. 3. Characterization of fibrotic and functional clusters. (a) Log-log plot of CCDF for a cluster size at  $\phi = 0.5$ . (b) Correlation length ( $\xi$ ) vs  $\phi$ . The dashed black line represents fibrotic and the blue lines the functional clusters at three values of  $e$ , respectively. Units of  $\xi$  and  $s$  are element edge length ( $0.25$  mm) and area ( $0.25$  mm) $^2$ , respectively.

as a power law with an exponential cutoff. However, for a given  $\phi$ , functional clusters tend to have larger sizes and cutoffs with a dependency on  $e$  (see Fig. S5 [5] for plots at different  $\phi$ 's). To quantitatively compare the system's characteristic cluster size at different  $\phi$  and  $e$ 's, we calculate the correlation length  $\xi$  using

$$\xi^2 = \frac{\sum_s 2R_s^2 s^2 n_s}{\sum_s s^2 n_s}, \quad (1)$$

where  $n_s$  is proportional to the number of clusters with size  $s$  and  $R_s$  is the cluster gyration radius [15] (see also Supplemental Material [5]). Figure 3(b) shows that  $\xi$  for functional clusters differs from that of the fibrotic clusters and that it is substantially affected by the excitability (e.g., at  $\phi = 0.5$ , we see an increase to 2.3-fold from fibrotic to functional clusters).

The statistical properties of functional clusters could also be used to explain the wave percolation phenomenon in the medium. We found that the percolation threshold, as calculated from the probability of formation of spanning (functional or fibrotic) clusters [15], closely matched the wave percolation threshold, as measured from the probability of formation of a total wave block in the medium (see Fig. S6 [5]). Importantly, here the functional clusters capture the dependency of percolation on the excitability (lower excitability results in a lower threshold due to a higher number of blocks), a fact that cannot be explained using the purely geometric fibrotic clusters. The percolation effect could also be inferred from the almost vertical curves in the plot of  $\xi$  in Fig. 3(b).

*Wave delays and minimal clusters.*—Our next step is to study the spatiotemporal aspects of rotational activity formation. If we consider this in the time domain, then following the occurrence of a unidirectional block, the tissue behind the block can be reexcited from the opposite direction if the propagation delay associated with the block ( $\tau$ ) is longer than the refractory period. The delay comes as a result of wave propagation around clusters to reach the conduction block from the opposite side. However, since multiple paths are possible for the wave front to reach there, it is reasonable to assume that the delay will be determined by the shortest path among the above paths. This motivates us to define the *minimal functional cluster* associated with a unidirectional block. This is determined by disconnecting the encompassing functional cluster at the location of the block and, among the resulting subclusters, finding the one that has the smallest perimeter ( $\Pi_{\min,f}$ ) (see also Supplemental Material [5]). The relevance of this definition is that the wave has to (partially or fully) travel along the boundary of the minimal functional cluster to reach the other side of the block and potentially cause reexcitation [Fig. 2(d)].

The distributions of  $\tau$  and  $\Pi_{\min,f}$  both show limited regions of linear regimes in the log-log plot, indicating

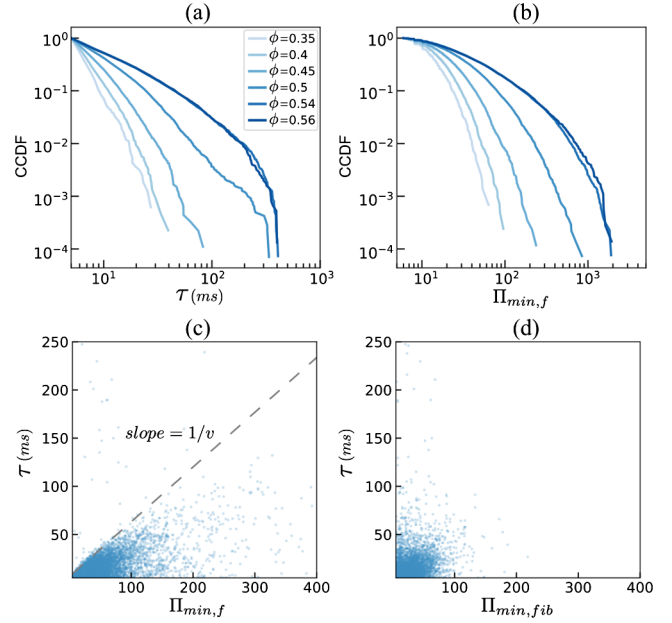


FIG. 4. Wave delays and minimal clusters. Log-log CCDF plots of (a) delays  $[\tau]$  and (b) minimal functional cluster perimeters  $[\Pi_{\min,f}]$  at different  $\phi$ 's (blue shades) and for  $e = 0.5$ . (c) Scatter plot of  $\tau$  vs  $\Pi_{\min,f}$  and (d)  $\tau$  vs  $\Pi_{\min,fib}$ , both at  $\phi = 0.5$  and  $e = 0.5$ . Unit of the perimeters is the element edge length (0.25 mm).

power-law behavior with a negative exponent and a cutoff [Figs. 4(a) and 4(b)]. If we study the pairwise relation of  $\tau$  vs  $\Pi_{\min,f}$ , we see that the graph has an upper envelope that is approximately a line with a slope of the inverse of wave velocity [Fig. 4(c)]. This indicates that the maximal delay occurs when the wave travels the full path around the minimal functional cluster. However, the majority of the points are below this line. This is reflective of the fact that, at the time of the conduction block, the wave front can touch the cluster at a point different from the block point, and, thus, it will have a shorter path to travel to the other side [Fig. 2(d)]. We can express such a path length ( $l$ ) as

$$l = \alpha \Pi_{\min,f}, \quad (2)$$

where  $\alpha$  is the fraction of the cluster perimeter that the reexcitation wave has to travel from the time of the block to reach the other side. Note that  $\alpha = 1$  corresponds to the case where the wave has to travel the full perimeter, but, in general,  $0 < \alpha \leq 1$ . Because of symmetry, it is reasonable to assume that on average the path will be half of the perimeter, which is equivalent to  $\alpha = 0.5$ . Equation (2) and this assumption are used in the next section to estimate the reentry probability.

In the above, we showed the physical correspondence between the minimal functional clusters and the wave delays that was also supported by the data. For comparison, we also calculated the minimal fibrotic cluster perimeter

( $\Pi_{\min, \text{fib}}$ ) by finding the smallest fibrotic cluster attached to a unidirectional block and studied its distribution (see Fig. S7 [5]). Notably, we see that a similar upper envelope does not exist in the plot of  $\tau$  vs  $\Pi_{\min, \text{fib}}$  [Fig. 4(d)]. This shows that minimal functional clusters significantly differ from their fibrotic counterparts and substantially better characterize the path of reexcitation.

*Probability of reentry formation.*—Finally, we will apply the concepts of minimal functional cluster and time delay to estimate the probability of reentry formation. As mentioned in the previous section, after the occurrence of a unidirectional block, the condition for the formation of reentry in the temporal domain is

$$\tau > t_r. \quad (3)$$

However, our main aim is to relate the formation of reentry to the geometric characteristics of the texture. We do this with the help of our definition of  $\Pi_{\min, f}$  and Eq. (2). We require that the path of the wave toward the block,  $l$ , is longer than the characteristic wavelength ( $\lambda = t_r \times v$ ), which leads to

$$\alpha \Pi_{\min, f} > \lambda, \quad (4)$$

where  $\lambda$  is calculated at  $\phi = 0$  for each  $e$ . Now, in order to estimate the probability in terms of minimal clusters only, we will assume  $\alpha = 0.5$  and estimate  $P(\alpha \Pi_{\min, f} > \lambda)$  accordingly. This assumption follows symmetry and represents on average a planar wave propagation. It is also compatible with the values of  $\alpha$  as measured from the data in Fig. 4(c), with  $\bar{\alpha} = 0.51$  and [1–99]th percentile of [0.12–0.99] (see Fig. S8 [5] for the histogram of  $\alpha$ ).

Figure 5(a) shows the results of the estimation of probability of reentry formation based on clusters and the comparison to empirical probabilities (at each point, the probability was estimated by applying the corresponding condition to a particular realization and averaging the binary results for  $N = 250$  realizations). We see that the condition based on the minimal functional cluster predicts the empirical probability of reentry with a high accuracy at different  $\phi$ 's and  $e$ 's [root-mean square error (RMSE) of 0.06]. It is also by far the best match when compared to other estimates of the probability based on different geometric features of the fibrotic clusters [Figs. 5(b)–5(d)]. For example, the estimation based on  $\Pi_{\min, \text{fib}}$  [Fig. 5(b)] greatly underestimates the probabilities and especially misses out on the chance of reentry formation at lower  $\phi$ 's. In contrast to the minimal clusters, the estimations that take into account all of the functional or fibrotic clusters in the tissue greatly overestimate the probabilities [Figs. 5(c) and 5(d)].

*Discussion.*—In this study, we demonstrated that the distribution of minimal functional cluster perimeter could accurately predict the reentry probability and its dependency on the fibrotic density and the tissue excitability. We

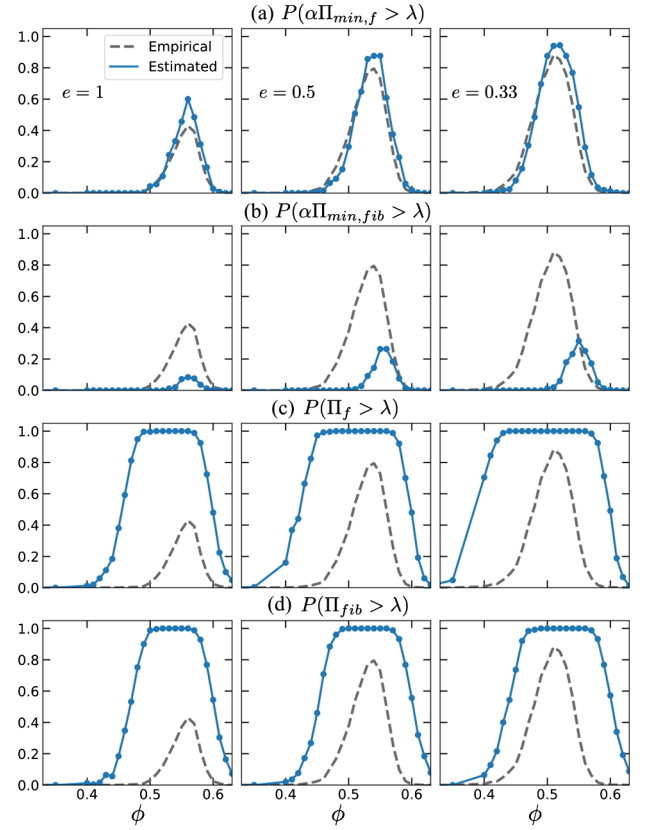


FIG. 5. Estimation of reentry probability as a function of  $\phi$  and  $e$ . Dashed line, empirical; solid line, estimated probabilities based on (a) minimal functional clusters, (b) minimal fibrotic clusters, (c) total functional clusters, and (d) total fibrotic clusters.  $\alpha = 0.5$  in (a) and (b). Probabilities were calculated from  $N = 250$  realizations. Average RMSE between the two curves are 0.06, 0.24, 0.54, and 0.46 for (a)–(d), respectively.

formulated this concept based on two ideas, the functional cluster and the minimal cluster, both of which we present here for the first time.

The functional cluster can be considered as a further development of the concept of a fibrotic cluster [12], since it takes into account not only the geometric properties of the texture, but also the properties of propagating waves, i.e., conduction blocks. We showed that its statistical properties, such as the size distribution and the percolation threshold, are a function of the excitability and substantially differ from those of fibrotic cluster. The idea of a minimal cluster, on the other hand, was developed on the basis of the theory of reentry and relates the local characteristic of unidirectional block essential for reentry initiation, with the global characteristic of reexcitation path required for reentry maintenance. We found that the combination of both concepts in the form of the minimal functional cluster most accurately predicted the probability of reentry. Indeed, if we considered only one of the above, either as minimal fibrotic clusters [Fig. 5(b)] or as total fibrotic or functional clusters [Figs. 5(c) and 5(d)], an underestimation or

overestimation of the probability was achieved, respectively. We speculate that the underestimation in the former case stems from the fact that it does not consider that the reentry could be formed around multiple connected smaller fibrotic clusters (functional clusters), while the overestimation in the latter model results from agnosticism to the occurrence of unidirectional blocks which is an additional requirement for reentry formation. The formalism of the minimal functional cluster addresses both of these issues.

The relationship between fibrosis texture and wave propagation has been addressed previously in many experimental and simulation studies. Such studies were devoted to various subjects, such as the relation between fibrosis and dynamic instabilities [16], wave propagation [17–19], onset of arrhythmias [20], or percolation [12,21,22]. Most of these studies addressed only qualitative effects of fibrosis or made associations using *ad hoc* features of the texture. It would be interesting to study whether the concept of functional cluster helps to explain any of the effects observed in those studies. In addition, direct comparisons to experiments could be made using cardiac heterocellular cocultures or optogenetics techniques [23,24]. In general, since our model is constructed from basic physical phenomena underlying the formation of reentry, we expect it to be widely applicable to different textures and various conditions of heterogeneity other than fibrosis.

Future work should be performed to expand and test the proposed concepts in more realistic scenarios. For example, anisotropy, 3D structure, or a more realistic cell connectivity could be incorporated [25–27]. Although we do not expect the main formalism of the model to change, we expect generalized definitions of some quantities such as the perimeter could be adopted. For example, the introduction of anisotropy could be studied using the Riemannian geometry framework of the wave propagation in the heart [28]. It would be interesting to see if the results obtained can also be applied to other excitable systems, such as chemical excitable media.

F.P. acknowledges support from the American Heart Association (18POST33990040). Research at Sechenov University (A. V. P.) was financed by the Ministry of Science and Higher Education of the Russian Federation within the framework of state support for creation and development of World-Class Research Center “Digital biodesign and personalized healthcare” No. 075-15-2020-926.

\*Corresponding author.

fpashak1@alumni.jh.edu

- [1] A. T. Winfree and S. H. Strogatz, Organizing centres for three-dimensional chemical waves, *Nature (London)* **311**, 611 (1984).  
 [2] G. R. Mines, On dynamic equilibrium in the heart, *J. Physiol.* **46**, 349 (1913).

- [3] T. P. Nguyen, Z. Qu, and J. N. Weiss, Cardiac fibrosis and arrhythmogenesis: The road to repair is paved with perils, *J. Mol. Cell. Cardiol.* **70**, 83 (2014).  
 [4] S. De Jong, T. A. van Veen, H. V. van Rijen, and J. M. de Bakker, Fibrosis and cardiac arrhythmias, *Journal of cardiovascular pharmacology* **57**, 630 (2011).  
 [5] See Supplemental Material at <http://link.aps.org/supplemental/10.1103/PhysRevLett.127.098101> for additional background, methods and results.  
 [6] A. G. Kléber and Y. Rudy, Basic mechanisms of cardiac impulse propagation and associated arrhythmias, *Physiol. Rev.* **84**, 431 (2004).  
 [7] J.-P. Drouhard and F. A. Roberge, Revised formulation of the Hodgkin-Huxley representation of the sodium current in cardiac cells, *Comput. Biomed. Res.* **20**, 333 (1987).  
 [8] G. W. Beeler and H. Reuter, Reconstruction of the action potential of ventricular myocardial fibres, *J. Physiol.* **268**, 177 (1977).  
 [9] T. Kawara, R. Derksen, J. R. de Groot, R. Coronel, S. Tasseron, A. C. Linnenbank, R. N. Hauer, H. Kirkels, M. J. Janse, and J. M. de Bakker, Activation delay after premature stimulation in chronically diseased human myocardium relates to the architecture of interstitial fibrosis, *Circulation* **104**, 3069 (2001).  
 [10] H. J. Arevalo, F. Vadakkumpadan, E. Guallar, A. Jebb, P. Malamas, K. C. Wu, and N. A. Trayanova, Arrhythmia risk stratification of patients after myocardial infarction using personalized heart models, *Nat. Commun.* **7**, 11437 (2016).  
 [11] N. Mewton, C. Y. Liu, P. Croisille, D. Bluemke, and J. A. Lima, Assessment of myocardial fibrosis with cardiovascular magnetic resonance, *J. Am. Coll. Cardiol.* **57**, 891 (2011).  
 [12] S. Alonso and M. Bär, Reentry near the Percolation Threshold in a Heterogeneous Discrete Model for Cardiac Tissue, *Phys. Rev. Lett.* **110**, 158101 (2013).  
 [13] G. Bub, A. Shrier, and L. Glass, Spiral Wave Generation in Heterogeneous Excitable Media, *Phys. Rev. Lett.* **88**, 058101 (2002).  
 [14] A modified Beeler-Reuter-Drouhard-Roberge ionic model was used for simulations with the CARPEntry package (Baseline parameters:  $v = 50$  cm/s,  $t_r = 60$  ms).  
 [15] D. Stauffer and A. Aharony, *Introduction to Percolation Theory* (Taylor & Francis, London, 1994).  
 [16] K. H. W. J. ten Tusscher and A. V. Panfilov, Influence of nonexcitable cells on spiral breakup in two-dimensional and three-dimensional excitable media, *Phys. Rev. E* **68**, 062902 (2003).  
 [17] A. Pertsov, Scale of geometric structures responsible for discontinuous propagation in myocardial tissue, in *Discontinuous Conduction in the Heart*, edited by P. M. Spooner, R. W. Joyner, and J. Jalife (Futura Publishing, Armonk, NY, 1997), p. 273–293.  
 [18] T. Nezhlobinsky, O. Solovyova, and A. Panfilov, Anisotropic conduction in the myocardium due to fibrosis: The effect of texture on wave propagation, *Sci. Rep.* **10**, 764 (2020).  
 [19] A. Dokuchaev, A. V. Panfilov, and O. Solovyova, Myocardial fibrosis in a 3d model: Effect of texture on wave propagation, *Mathematics* **8**, 1352 (2020).  
 [20] I. V. Kazbanov, K. H. Ten Tusscher, and A. V. Panfilov, Effects of heterogeneous diffuse fibrosis on arrhythmia dynamics and mechanism, *Sci. Rep.* **6**, 20835 (2016).

- [21] S. Alonso, R. W. dos Santos, and M. Bär, Reentry and ectopic pacemakers emerge in a three-dimensional model for a slab of cardiac tissue with diffuse microfibrosis near the percolation threshold, *PLoS One* **11**, e0166972 (2016).
- [22] E. Vigmond, A. Pashaie, S. Amraoui, H. Cochet, and M. Hassaguerre, Percolation as a mechanism to explain atrial fractionated electrograms and reentry in a fibrosis model based on imaging data, *Heart Rhythm* **13**, 1536 (2016).
- [23] S. Zlochiver, V. Munoz, K. L. Vikstrom, S. M. Taffet, O. Berenfeld, and J. Jalife, Electrotonic myofibroblast-to-myocyte coupling increases propensity to reentrant arrhythmias in two-dimensional cardiac monolayers, *Biophys. J.* **95**, 4469 (2008).
- [24] R. Majumder, I. Feola, A. S. Teplenin, A. A. De Vries, A. V. Panfilov, and D. A. Pijnappels, Optogenetics enables real-time spatiotemporal control over spiral wave dynamics in an excitable cardiac system, *eLife* **7**, e41076 (2018).
- [25] N. Kudryashova, A. Nizamieva, V. Tsvelaya, A. V. Panfilov, and K. I. Agladze, Self-organization of conducting pathways explains electrical wave propagation in cardiac tissues with high fraction of non-conducting cells, *PLoS Comput. Biol.* **15**, e1006597 (2019).
- [26] V. Jacquemet and C. S. Henriquez, Genesis of complex fractionated atrial electrograms in zones of slow conduction: A computer model of microfibrosis, *Heart Rhythm* **6**, 803 (2009).
- [27] S. L. Rutherford, M. L. Trew, G. B. Sands, I. J. LeGrice, and B. H. Smaill, High-resolution 3-dimensional reconstruction of the infarct border zone: Impact of structural remodeling on electrical activation, *Circ. Res.* **111**, 301 (2012).
- [28] R. J. Young and A. V. Panfilov, Anisotropy of wave propagation in the heart can be modeled by a riemannian electrophysiological metric, *Proc. Natl. Acad. Sci. U.S.A.* **107**, 15063 (2010).